Article

Catalytically Active □-Oxodiiron(IV) Oxidants from Iron(III) and Dioxygen

Anindya Ghosh, Filipe Tiago de Oliveira, Toshihiro Yano, Takanori Nishioka, Evan S. Beach, Isamu Kinoshita, Eckard Mnck, Alexander D. Ryabov, Colin P. Horwitz, and Terrence J. Collins

J. Am. Chem. Soc., **2005**, 127 (8), 2505-2513• DOI: 10.1021/ja0460458 • Publication Date (Web): 03 February 2005

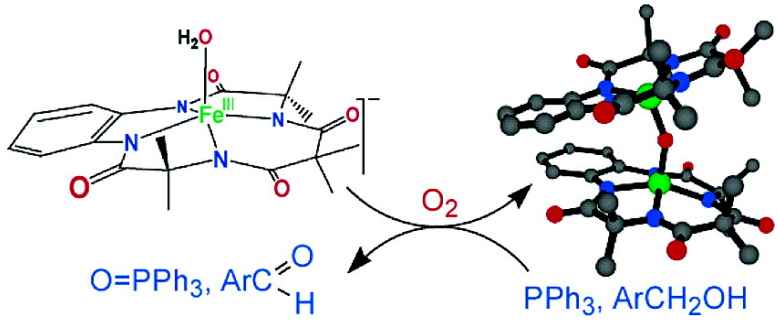

More About This Article

Additional resources and features associated with this article are available within the HTML version:

- Supporting Information
- Links to the 15 articles that cite this article, as of the time of this article download
- Access to high resolution figures
- Links to articles and content related to this article
- Copyright permission to reproduce figures and/or text from this article

View the Full Text HTML

J|A|C|S
ARTICLES
Published on Web 02/03/2005

Catalytically Active μ-Oxodiiron(IV) Oxidants from Iron(III) and Dioxygen

Anindya Ghosh,[†] Filipe Tiago de Oliveira,[†] Toshihiro Yano,[‡] Takanori Nishioka,[‡] Evan S. Beach,[†] Isamu Kinoshita,*[,‡] Eckard Münck,*[,†] Alexander D. Ryabov,[†] Colin P. Horwitz,[†] and Terrence J. Collins*[,†]

Contribution from the Department of Chemistry, Carnegie Mellon University, Pittsburgh, Pennsylvania 15213, Molecular Materials Science Department, Graduate School of Science, Osaka City University, 3-3-138 Sugimoto Sumiyoshi, Osaka 5588585, Japan

Received July 2, 2004; E-mail: tc1u@andrew.cmu.edu

Abstract: The reaction between an Fe^{III} complex and O_2 to afford a stable catalytically active diiron(IV)-μ-oxo compound is described. Phosphonium salts of orange five-coordinated Fe^{III}−TAML complexes with an axial aqua ligand ([PPh_4]**1**−H_2O, tetraamidato macrocyclic Fe^{III} species derived from 3,3,6,6,9,9-hexamethyl-3,4,8,9-tetrahydro-1*H*-1,4,8,11-benzotetraazacyclotridecine-2,5,7,10(6*H*,11*H*)-tetraone) react rapidly with O_2 in CH_2Cl_2 or other weakly coordinating solvents to produce black μ-oxo-bridged diiron(IV) complexes, **2**, in high yields. Complexes **2** have been characterized by X-ray crystallography (2 cases), microanalytical data, mass spectrometry, UV/Vis, Mössbauer, and ^{1}H NMR spectroscopies. Mössbauer data show that the diamagnetic Fe−O−Fe unit contains antiferromagnetically coupled $S = 1$ Fe^{IV} sites; diamagnetic ^{1}H NMR spectra are observed. The oxidation of PPh_3 to $OPPh_3$ by **2** was confirmed by UV/Vis and GC−MS. Labeling experiments with $^{18}O_2$ and $H_2{}^{18}O$ established that the bridging oxygen atom of **2** derives from O_2. Complexes **2** catalyze the selective oxidation of benzylic alcohols into the corresponding aldehydes and bleach rapidly organic dyes, such as Orange II in MeCN−H_2O mixtures; reactivity evidence suggests that free radical autoxidation is not involved. This work highlights a promising development for the advancement of green oxidation technology, as O_2 is an abundant, clean, and inexpensive oxidizing agent.

Introduction

Dioxygen (O_2) is the principal oxidizing agent of aerobic biochemistry. It is abundant and inexpensive. Its interactions with enzymes are an integral part of evolution for aerobic organisms. Persistent bioaccumulative toxicants are therefore rarely produced through biochemical oxidations. This marks a key difference from technologically prevalent metal- and chlorine-based oxidations and highlights the importance of developing useful O_2-activating catalysts in the pursuit of sustainable oxidation technologies.[1]

Biochemical oxidations by dioxygen have been broadly studied for many decades. Reactions involving iron(IV) intermediates have often been demonstrated for iron heme enzymes where O_2 interacts with iron(II) and not iron(III).[2−9] High-valent iron−oxo species are the key reactive intermediates. One such intermediate is known as compound I, a porphyrin radical cation iron(IV)−oxo species, which is observed, among others, in cytochrome P450 catalytic cycles. For the P450 enzymes, compound I species are produced following the binding of O_2 to the ferrous heme intermediate.[10−13] Non-heme iron enzymes also activate O_2 at the ferrous state.[14−19] Iron(IV)oxo species derived from Fe^{II} and O_2 have been postulated as oxidizing agents for non-heme mononuclear iron(II) enzymes that require pterin or α-ketoglutarate cofactors.[15] Price et al. have recently

[†] Carnegie Mellon University.
[‡] Osaka City University.

(1) Collins, T. J. *Science* **2001**, *291*, 48−49.
(2) Pond, A. E.; Ledbetter, A. P.; Sono, M.; Goodin, D. B.; Dawson, J. H. In *Electron Transfer in Chemistry*; Balzani, V., Ed.; Wiley-VCH Verlag GmbH: Weinheim, Germany, 2001; Vol. 3, pp 56−104.
(3) Meunier, B.; Bernadou, J. *Struct. Bonding* **2000**, *97*, 1−35.
(4) Ortiz de Montellano, P. R.; De Voss, J. J. *Nat. Prod. Rep.* **2002**, *19*, 477−493.
(5) Groves, J. T. *Proc. Natl. Acad. Sci. U.S.A.* **2003**, *100*, 3569−3574.
(6) Malmström, B. G. In *Electron Transfer in Chemistry*; Balzani, V., Ed.; Wiley-VCH Verlag GmbH: Weinheim, Germany, 2001; Vol. 3, pp 39−55.
(7) Durham, B.; Millet, F. S. In *Encyclopedia of Inorganic Chemistry*; King, R. B., Ed.; Wiley & Sons Ltd.: New York, 1994; p 1642.
(8) Groves, J. T.; Wang, C. C.-Y. *Curr. Opin. Chem. Biol.* **2000**, *4*, 687−695.
(9) Stuehr, D. J. *Annu. Rev. Pharmacol. Toxicol.* **1997**, *37*, 339−359.
(10) Schlichting, I.; Berendzen, J.; Chu, K.; Stock, A. M.; Maves, S. A.; Benson, D. E.; Sweet, R. M.; Ringe, D.; Petsko, G. A.; Sligar, S. G. *Science* **2000**, *287*, 1615−1622.
(11) Kellner, D. G.; Hung, S.-C.; Weiss, K. E.; Sligar, S. G. *J. Biol. Chem.* **2002**, *277*, 9641.
(12) Harris, d. L.; Loew, G. H. *J. Am. Chem. Soc.* **1998**, *120*, 8941−8948.
(13) Ogliaro, F.; de Visser, S. P.; Cohen, S.; Sharma, P. K.; Shaik, S. *J. Am. Chem. Soc.* **2002**, *124*, 2806−2817.
(14) Costas, M.; Mehn, M. P.; Jensen, M. P.; Que, L., Jr. *Chem. Rev.* **2004**, *104*, 939−986.
(15) Solomon, E. I.; Brunold, T. C.; Davis, M. I.; Kemsley, J. N.; Lee, S.-K.; Lehnert, N.; Neese, F.; Skulan, A. J.; Yang, Y.-S.; Zhou, J. *Chem. Rev.* **2000**, *100*, 235−349.
(16) Funabiki, T. In *Catalysis by Metal Complexes*; Funabiki, T., Ed.; Kluwer Academic Publishers: Dordrecht/Boston/London, 1996; Vol. 19, pp 1−393.
(17) Wallar, B. J.; Lipscomb, J. D. *Chem. Rev.* **1996**, *96*, 2625−2657.
(18) Westerheide, L.; Matthias, P.; Krebs, B. *Curr. Opin. Chem. Biol.* **2000**, *4*, 235−241.
(19) Baik, M.-H.; Newcomb, M.; Friesner, R. A.; Lippard, S. J. *Chem. Rev.* **2003**, *103*, 2385−2419.

reported on the Fe^{IV} intermediate for α-ketoglutarate-dependent dioxygenase studied by the Mössbauer spectroscopy.[20] As illustrated by the subtlety of iron−oxo chemistry, this intermediate contains high-spin Fe^{IV} ($S = 2$), in contrast with the intermediate-spin Fe^{IV} ($S = 1$) species encountered in heme proteins. The non-heme diiron methane monooxygenase enzyme reacts with O_2 in its Fe^{II} state to form the bis[(μ-oxo)iron(IV)] reactive intermediate known as compound Q.[21,22]

The biomimetic oxidation chemistry of synthetic iron porphyrins[23,24] and non-heme iron complexes[14,16,25−28] has also been widely investigated. Several classic studies are particularly relevant to the work reported here. Balch et al. established a mechanism for the ubiquitous reaction between sterically nonprotected Fe^{II}−porphyrins and dioxygen, specifically, the rapid formation of bis(Fe^{III}porphyrin)-μ-oxo dimers where bis-(Fe^{III}porphyrin)-μ-peroxo and (Fe^{IV}porphyrin)oxo complexes are key intermediates.[29−32] Non-heme diiron(II) enzyme mimics have been proposed to interact with O_2 to generate dinuclear mixed valent Fe^{III}/Fe^{IV} oxo-bridged dinuclear species.[33−35] In each of these examples, as with the enzymes and the biological oxygen carriers, dioxygen interacts with iron(II) and not with iron(III). As one ambiguity, Fe^{III}−catecholate compounds, used as models of catechol dioxygenases, react with dioxygen to produce catalytic aromatic ring cleavage. One component of the proposed mechanism involves direct interaction between iron and O_2. However, the electronic structure is thought to be comprised of contributions from Fe^{III}−catecholate and Fe^{II}−catecholate radicals such that this process is not a clear example of a coordination reaction between iron(III) and O_2.[16,36,37]

The above biochemical and biomimetic studies highlight the ongoing need for synthetic iron compounds that can produce technologically useful O_2 activation chemistry. Over the last two decades, we have developed oxidatively robust iron(III) complexes, referred to as Fe−TAML activators (**1**−H_2O, Scheme 1), that catalyze a variety of technologically important oxidations by hydrogen peroxide in water.[38,39] These include

Scheme 1. Principal Compounds of This Study

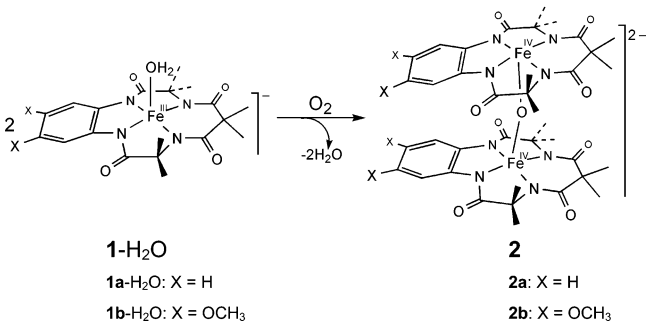

1-H_2O **2**

1a-H_2O: X = H **2a**: X = H

1b-H_2O: X = OCH_3 **2b**: X = OCH_3

the rapid bleaching of water-soluble dyes,[40] the decolorization of pulp mill effluents, the delignification of wood pulp,[41] the complete remediation of chlorophenol persistent pollutants,[42] and the selective oxidation of thiophene compounds of gasoline and diesel.[43] High-valent iron−oxo species are presumably involved in these oxidations.[44] However, if TAML activators could be shown to activate dioxygen via the formation of high-valent iron−oxo complexes, their potential utility would be expanded.

The results reported here highlight the capability of Fe^{III}−TAMLs to activate O_2 under mild conditions via nonfree radical processes. Particularly, we report on (1) the unprecedented homogeneous reaction between Fe^{III} complexes [PPh_4]**1**−H_2O[45] with O_2 to generate Fe^{IV}−O−Fe^{IV} complexes, **2** (Scheme 1), (2) isolation and full characterization of complexes **2**, and (3) the reactivity of **2** toward organic substrates, such as alcohols. Mechanistic pathways are also discussed.

Experimental Section

General Considerations. All reagents and solvents were purchased from commercial sources and were used as received, unless otherwise noted. Orange II was purified via chromatography using a C18 silica column. Cumene (isopropylbenzene) was passed through an alumina column under an inert atmosphere to remove impurities. All of the tetraamido macrocyclic ligands (TAML) were prepared according to described procedures.[46] Solvents were dried according to published

(20) Price, J. C.; Barr, E. W.; Tirupati, B.; Bollinger, J. M. J.; Krebs, C. *Biochemistry* **2003**, *42*, 7497−7508.
(21) Lee, S.-K.; Fox, B. G.; Froland, W. A.; Lipscomb, J. D.; Münck, E. *J. Am. Chem. Soc.* **1993**, *115*, 6450−6451.
(22) Shu, L.; Nesheim, J. C.; Kauffmann, K. E.; Münck, E.; Lipscomb, J. D.; Que, L., Jr. *Science* **1997**, *275*, 515−518.
(23) Watanabe, Y. In *Model Studies on Heme Monooxygenases*; Funabiki, T., Ed.; Kluwer Academic Publishers: Dordrecht/Boston/London, 1996; Vol. 19, pp 223−282.
(24) Watanbe, Y.; Fujji, H. *Struct. Bonding* **2000**, *97*, 61−89.
(25) Funabiki, T. In *Catalysis by Metal Complexes (Advances in Catalytic Activation of Dioxygen by Metal Complexes)*; Simandi, L. I., Ed.; Kluwer Academic Publishers: Dordrecht/Boston/London, 2003; Vol. 26, pp 157−226.
(26) Rohde, J.-U.; Bukowski, M. R.; Que, L., Jr. *Curr. Opin. Chem. Biol.* **2003**, *7*, 674−682.
(27) Simandi, L. I.; Simandi, T. M.; May, Z.; Besenyei, G. *Coord. Chem. Rev.* **2003**, *245*, 85−93.
(28) MacBeth, C. E.; Golombek, A. P.; Young, V. G., Jr.; Yang, C.; Kuczera, K.; Hendrich, M. P.; Borovik, A. S. *Science* **2000**, *289*, 938−941.
(29) Chin, D.-H.; La Mar, G. N.; Balch, A. L. *J. Am. Chem. Soc.* **1980**, *102*, 4344−4350.
(30) Balch, A. L.; Chan, Y. W.; Cheng, R. J.; La Mar, G. N.; Latos-Grazynski, L.; Renner, M. W. *J. Am. Chem. Soc.* **1984**, *106*, 7779−7785.
(31) Chin, D.-H.; La Mar, G. N.; Balch, A. L. *J. Am. Chem. Soc.* **1980**, *102*, 5945−5947.
(32) Chin, D.-H.; Balch, A. L.; La Mar, G. N. *J. Am. Chem. Soc.* **1980**, *102*, 1446−1448.
(33) MacMurdo, V. L.; Zheng, H.; Que, L., Jr. *Inorg. Chem.* **2000**, *39*, 2254−2255.
(34) Lee, D.; Du Bois, J.; Petasis, D.; Hendrich, M. P.; Krebs, C.; Huynh, B. H.; Lippard, S. J. *J. Am. Chem. Soc.* **1999**, *121*, 9893−9894.
(35) Lee, D.; Pierce, B.; Krebs, C.; Hendrich, M. P.; Huynh, B. H.; Lippard, S. J. *J. Am. Chem. Soc.* **2002**, *124*, 3993−4007.
(36) Funabiki, T.; Yamazaki, T. J. *J. Mol. Catal. A* **1999**, *150*, 37−47.
(37) Jo, D.-H.; Que, L., Jr. *Angew. Chem., Int. Ed.* **2000**, *39*, 4284−4287.
(38) Collins, T. J. *Acc. Chem. Res.* **1994**, *27*, 279−285.
(39) Collins, T. J. *Acc. Chem. Res.* **2002**, *35*, 782−790.
(40) Horwitz, C. P.; Fooksman, D. R.; Vuocolo, L. D.; Gordon-Wylie, S. W.; Cox, N. J.; Collins, T. J. *J. Am. Chem. Soc.* **1998**, *120*, 4867−4868.
(41) *TAML® Catalytic Oxidant Activators in the Pulp and Paper Industry*; Collins, T. J.; Horwitz, C. P.; Ryabov, A. D.; Vuocolo, L. D.; Sen Gupta, S.; Ghosh, A.; Fattaleh, N. L.; Hangun, Y.; Steinhoff, B.; Noser, C. A.; Beach, E.; Prasuhn, D., Jr.; Stuthridge, T.; Wingate, K. G.; Hall, J.; Wright, L. J.; Suckling, I.; Allison, R. W. ACS Symposium Series 823; American Chemical Society: Washington, DC, 2002; 47−60.
(42) Sen Gupta, S.; Stadler, M.; Noser, C. A.; Ghosh, A.; Steinhoff, B.; Lenoir, D.; Horwitz, C. P.; Schramm, K.-W.; Collins, T. J. *Science* **2002**, *296*, 326−328.
(43) Hangun, Y.; Alexandrova, L.; Khetan, S.; Horwitz, C. P.; Cugini, A.; Link, D. D.; Howard, B.; Collins, T. J. *Preprints − ACS, Div. Petro. Chem.* **2002**, *47*, 42−44.
(44) High-valent Fe^{IV}−TAML complexes have been generated by using Ce^{IV} or *tert*-BuOOH, but these non-oxo species generated in nonaqueous medium are catalytically irrelevant and not involved in the oxidations by H_2O_2 in water: (a) Collins, T. J.; Kostka, K. L.; Münck, E.; Uffelman, E. S. *J. Am. Chem. Soc.* **1990**, *112*, 5637−5639. (b) Kostka, K. L.; Fox, B. G.; Hendrich, M. P.; Collins, T. J.; Rickard, C. E. F.; Wright, L. J.; Münck, E. *J. Am. Chem. Soc.* **1993**, *115*, 6746−6757. (c) Bartos, M. J.; Gordon-Wylie, S. W.; Fox, B. G.; Wright, L. J.; Weintraub, S. T.; Kauffmann, K. E.; Münck, E.; Kostka, K. L.; Uffelman, E. S.; Rickard, C. E. F.; Noon, K. R.; Collins, T. J. *Coord. Chem. Rev.* **1998**, *174*, 361−390.
(45) Ghosh, A.; Ryabov, A. D.; Mayer, S. M.; Horner, D. C.; Prasuhn, D. E., Jr.; Sen Gupta, S.; Vuocolo, L. D.; Culver, C.; Hendrich, M. P.; Rickard, C. E. F.; Norman, R. E.; Horwitz, C. P.; Collins, T. J. *J. Am. Chem. Soc.* **2003**, *125*, 12378−12379.
(46) Patents of the Collins group, including the key experimental procedures at http://www.chem.cmu.edu/groups/collins/awardpatpub/patents/index.html.

procedures,[47] distilled, and stored under argon or nitrogen. $^{18}O_2$ (89−90%) and $H_2{}^{18}O$ (95%) were purchased from Cambridge Isotope Laboratories, Inc. Preparation and handling of air-sensitive materials were performed under an inert atmosphere by using either Schlenk and vacuum line techniques or a glovebox. Elemental analyses were performed by Midwest Microlab.

Physical Methods. UV/Vis spectra were recorded on an HP 8453 diode array spectrophotometer. ESI-MS was performed on a Thermo Finnigan LCQ quadrupole field mass spectrometer with electrospray ionization. GC−MS analyses were performed using a Hewlett-Packard 6890/5973 network system (He carrier gas, HP-5MS cross-linked 5% PH ME siloxane column, electron impact ionization at 70 eV). Cyclic voltammetry was performed using an EG&G PARC electrochemical analysis system (Model 263A) in dichloromethane under a nitrogen atmosphere, using a conventional three-electrode configuration. A glassy carbon electrode (3 mm diameter) was used as working electrode. The ferrocene−ferricenium reference couple gave a peak separation of 110 mV at a scan rate of 50 mV s^{-1}. ^{1}H NMR spectra were recorded in CD_2Cl_2 at 300 K on a Bruker Avance AV 300 MHz spectrometer; chemical shifts in δ are reported versus tetramethylsilane.

X-ray Crystallographic Studies of 2a and 2b. A black prism-shaped crystal of **2a** (0.40 × 0.20 × 0.15 mm) or a red prismatic crystal of **2b** (0.15 × 0.15 × 0.20 mm) was placed onto a glass fiber mounted on a Rigaku/MSC Mercury CCD diffractometer (graphite-monochromated Mo Kα radiation (λ = 0.71069 Å)). Data collection and processing were performed using the Rigaku/MSC CrystalClear program. The structures were solved by using SIR92[48] direct method and expanded using Fourier techniques. The full-matrix refinements were performed using SHELXL-97[49] and teXsan[50] as a graphical interface. All non-hydrogen atoms were refined with anisotropic displacement parameters. All hydrogen atoms were found in the difference Fourier map and refined isotropically for **2a** or as riding models for **2b**. For **2a**, the weighting scheme $w = [\sigma^2(F_o^2) + \{0.0001 \times (F_o^2 + 2F_c^2)/3\}^2]^{-1}$ was employed. For **2a**, the final $R_1 = (\Sigma||F_o| - |F_c||/\Sigma|F_o|)$ for the observed data, $wR_2 = (\{\Sigma w(F_o^2 - F_c^2)^2/\Sigma w(F_o^2)^2\}^{1/2})$ for all data, and GOF = $([\Sigma\, w(F_o^2 - F_c^2)^2/(N_o - N_v)]^{1/2})$ were 0.0532, 0.0765, and 1.042, respectively. Additional information on the crystal data and refinement is given in Table 1.

Mössbauer Spectroscopy. Mössbauer spectra were recorded with two spectrometers using Janis Research (Wilmington, MA) Super-Varitemp dewars that allow studies in applied magnetic fields up to 8.0 T in the temperature range from 1.5 to 200 K. Spectral simulations were performed using the WMOSS software package (WEB Research, Minneapolis). Isomer shifts are quoted relative to Fe metal at 298 K. Solid samples of **2a** and **2b** were prepared by reaction of [PPh_4]**1a**−H_2O and [PPh_4]**1b**−H_2O with O_2 in CH_2Cl_2 followed by recrystallization from a mixture of CH_2Cl_2/α,α,α-trifluorotoluene. To prevent movement, polycrystalline powders of **2a** and **2b** (0.1 g each) were suspended in mineral oil (1 mL).

Synthesis of [PPh_4]1a−H_2O.[45] [Li]**1a**−H_2O (0.5 g, 1.06 mmol) was dissolved in deionized water (5 mL), and the solution was filtered. A solution of [PPh_4]Cl (2.1 g, 5.6 mmol) in water (10 mL) was added dropwise to the solution of [Li]**1a**−H_2O with stirring to produce a reddish precipitate. The solid was recrystallized from acetonitrile−water (1:1, v/v). The resulting orange crystalline material was dried in a vacuum oven for 5 h at 45 °C. Yield 83%. Anal. Calcd for $C_{43}H_{42}N_4PO_4Fe{\cdot}3H_2O$: C, 63.00; H, 5.90; N, 6.83. Found: C, 62.80; H, 5.78; N, 6.81. ESI-MS: *m*/*z* 426 (calcd for **1a** 426).

Synthesis of [PPh_4]1b−H_2O. Dark red [PPh_4]**1b**−H_2O was synthesized in a fashion similar to that of [PPh_4]**1a**−H_2O. Yield 85%. Anal. Calcd for $C_{45}H_{46}N_4PO_6Fe{\cdot}2H_2O$: C, 62.72; H, 5.84; N, 6.50. Found: C, 62.65; H, 5.90; N, 6.37. ESI-MS: *m*/*z* 486 (calcd for **1b** 486).

Table 1. Crystallographic Data, Experimental Conditions, and Refinement Details for **2a** and **2b**

crystal data	2a	2b
chemical formula	$C_{86}H_{86}Fe_2N_8O_{10}P_2$	$C_{97}H_{98}F_3Fe_2N_8O_{13.5}P_2$
*F*w	1565.31	1822.52
crystal system	monoclinic	triclinic
space group	*C*2/*c* (No. 15)	*P*1 (No. 2)
a (Å)	13.649(3)	14.084(1)
b (Å)	25.077(5)	15.380(2)
c (Å)	22.742(4)	24.082(2)
α (deg)	90	97.723(8)
β (deg)	91.952 (4)	100.09(1)
γ (deg)	90	117.146(6)
V (Å^3)	7779 (2)	4431.4(9)
Z	4	2
D_{cal} (g cm^{-3})	1.336	1.366
temp (K)	193(1)	193(1)
μ (Mo Kα) (cm^{-1})	4.79	4.39
reflections collected	38058	43675
independent reflections	8740 (R_{int} = 0.074)	19233 (R_{int} = 0.045)
$T_{min} - T_{max}$	0.8887−0.9673	0.9250−0.9558
data/parameter	8740/660	19233/1459
R_1 [$I > 2\sigma(I)$]	0.0532	0.0628
wR_2 (all data)	0.0765	0.1618
GOF	1.042	1.078
$\Delta\rho$ (e Å^{-3})	min −0.35, max 0.56	min −0.45, max 0.41

Synthesis of 2a. [PPh_4]**1a**−H_2O (0.1 g, 0.13 mmol) was dissolved in dichloromethane (3 mL) and stirred under either air or a dry oxygen atmosphere for 10 min. Dry α,α,α-trifluorotoluene (1.5 mL) was then added to the resulting black solution which was allowed to stand in an open vial at room temperature for 6 h to yield black prismatic crystals. These were collected by filtration and dried under vacuum. Yield 82%. Anal. Calcd for $C_{86}H_{84}Fe_2N_8O_9P_2{\cdot}2H_2O$: C, 65.24; H, 5.60; N, 7.08. Found: C, 65.30; H, 5.46; N, 7.01. ESI-MS revealed two fragments of equal intensity: *m*/*z* 426 (calcd for **1a** 426), and *m*/*z* 442 (calcd for **1a**(O) 442) (Figure 5). ^{1}H NMR (CD_2Cl_2, 300 MHz, δ): 1.18 (s, 6 H, diastereotopic CH_3 six-membered rings), 1.23 (s, 6 H, diastereotopic CH_3 six-membered rings), 1.36 (s, 12 H, diastereotopic CH_3 five-membered rings), 1.79 (s, 12 H, diastereotopic CH_3 five-membered rings), 7.23 (m, 4 H, macrocyclic ArH), 7.57−7.85 (m, PPh_4^+), 8.27 (m, 4 H, macrocyclic ArH).

Synthesis of 2b. Compound **2b** was synthesized similarly to **2a**. Yield 89%. Anal. Calcd for $C_{90}H_{92}Fe_2N_8O_{13}P_2{\cdot}C_7H_5F_3{\cdot}H_2O$: C, 63.61; H, 5.44; N, 6.11. Found: C, 63.61; H, 5.44; N, 6.11. ESI-MS revealed two fragments of equal intensity: *m*/*z* 486 (calcd for **1b** 486), and *m*/*z* 502 (calcd for **1b**(O) 502). ^{1}H NMR (CD_2Cl_2, 300 MHz, δ): 1.18 (s, 6 H, diastereotopic CH_3 six-membered rings), 1.20 (s, 6 H, diastereotopic CH_3 six-membered rings), 1.42 (s, 12 H, diastereotopic CH_3 five-membered rings), 1.74 (s, 12 H, diastereotopic CH_3 five-membered rings), 3.70 (s, 12 H, OCH_3) 7.54−7.86 (m, macrocyclic ArH, PPh_4^+, $CF_3C_6H_5$).

Titration of 2a with PPh_3 and Decamethylferrocene (Cp^*_2Fe). A solution of **2a** in CH_2Cl_2 (0.92 mM) was titrated with PPh_3 dissolved in CH_2Cl_2 (2.3 mM). Aliquots of PPh_3 were added to the solution of **2a**, and the UV/Vis spectral changes were recorded after each addition. Correction for dilution was applied. Spectral changes at 542 nm were plotted against the added [PPh_3]. Similarly, a CH_2Cl_2 solution of **2a** (typically 0.109 mM) was subjected to titration with Cp^*_2Fe dissolved in CH_2Cl_2 (3.04 mM). Aliquots of Cp^*_2Fe were delivered to the solution under argon using a gastight syringe; **2a** was found to react rapidly with Cp^*_2Fe. Spectral changes at 542 nm were plotted against the added [Cp^*_2Fe] (Figure S2 in the Supporting Information).

Reaction of $^{18}O_2$ with [PPh_4]1a−H_2O To Generate ^{18}O-Enriched 2a. [PPh_4]**1a**−H_2O (0.01 g, 1.27 × 10^{-2} mmol) was dissolved in dry degassed dichloromethane (10 mL) at room temperature. Excess gaseous

(47) Armarego, W. L. F.; Perrin, D. D. *Purification of Laboratory Chemicals*, 4th ed.; Pergamon Press: Oxford, 1997.
(48) Altomare, A.; Burla, M. C.; Camalli, M.; Cascarano, M.; Giacovazzo, C.; Guagliardi, A.; Polidori, G. *J. Appl. Crystallogr.* **1994**, *27*, 435−436.
(49) Sheldrick, G. M. *SHELXL-97*, Program for the Refinement of Crystal Structures; University of Göttingen: Göttingen, Germany, 1997.
(50) *teXsan: Structure Analysis Package*, Molecular Structure Corporation, 1985 and 1999.

$^{18}O_2$ (89−90%) was then admitted, and the solution was stirred for 10 min. The solution color changed from red to black. A portion of the reaction mixture was injected into the ESI mass spectrometer to ascertain the degree of ^{18}O incorporation (Figure S3 in the Supporting Information). Enrichment by the ^{18}O isotope was observed for **1a**(O). PPh_3 (6 mg, 2.3×10^{-2} mmol) was then added under argon to the solution, and the mixture was stirred at room temperature for 5 min. The black solution turned orange. GC−MS was employed to quantify the $^{18}OPPh_3$ (53% ^{18}O incorporation).

Reaction of $^{18}O_2$ with [PPh_4]1a−$H_2{}^{18}O$. [PPh_4]**1a**−H_2O (21 mg, 26.8 μmol) was dissolved in dry acetonitrile (5 mL), and the solution was stirred for 12 h in the presence of $H_2{}^{18}O$ (95%, 50 μL, 2.8 mmol). The solvent was removed under reduced pressure, and the orange solid dried for 6 h in vacuum. The residual material was then dissolved in degassed CH_2Cl_2 (5 mL), and $^{18}O_2$ gas was bubbled through the reaction mixture. After addition of PPh_3 (9 mg, 34 μmol), the solution was stirred for 10 min, and then the reaction mixture was analyzed by GC−MS (Figure S4 in the Supporting Information) to quantify the formation of $^{18}OPPh_3$ (86% incorporation).

Reaction of [PPh_4]1a−$H_2{}^{18}O$ with $^{16}O_2$. [PPh_4]**1a**−$H_2{}^{18}O$ (5 mg, 6.38 μmol) was prepared following the method described above. The orange solid was dissolved in dry degassed CH_2Cl_2 (5 mL), and $^{16}O_2$ was added to the reaction mixture, producing a black solution. ESI-MS of the reaction solution showed 44% ^{18}O enrichment of **1a**(O) (Figure S5 in the Supporting Information).

Reaction of 2a with $H_2{}^{18}O$. Compound **2a** produced from $^{16}O_2$ (21 mg, 13.3 μmol) was dissolved in dry CH_2Cl_2 (5 mL) and stirred with $H_2{}^{18}O$ (95%, 25 μL, 1.38 mmol) for 3 h. The solvent was removed, and the solid was dried under vacuum at 40 °C (24 h). This ^{18}O-exchanged **2a** was then dissolved in CH_2Cl_2 (5 mL); PPh_3 (3 mg, 11.4 μmol) was added, and the solution was stirred for 5 min. The reaction mixture was analyzed by GC−MS (Figure S7 in the Supporting Information) to determine the formation of $^{18}OPPh_3$ (73% incorporation).

Reaction of 2a with Benzyl, 4-Chlorobenzyl, 4-Nitrobenzyl, 4-Methoxybenzyl, and Cinnamyl Alcohols. The reaction conditions used were similar for all alcohols as described below. Compound **2a** (10 mg, 6.3 μmol) was dissolved in 1,2-dichlorobenzene (2 mL). The reaction mixture was slowly heated to 100 °C. Benzyl alcohol (96 μmol) was added with stirring. After 5 min, GC−MS analysis of the reaction mixture showed the formation of benzaldehyde. Several portions of the alcohol (96 μmol each time) were added over 1 h while bubbling air into the reaction mixture; a total of 0.60 mmol of benzyl alcohol was added; 60 of the 95 equivalents of added alcohol relative to **2a** were converted to benzaldehyde. Benzoic acid was not observed by the GC−MS experiment. The reaction medium was treated with $[(CH_3)_3S](OH)$,[51] and no methyl benzoate was observed by GC−MS.

Generation of 2a in the Presence of Cumene. To probe the involvement of radical processes in the formation of **2a**, its synthesis was performed in the presence of cumene. [PPh_4]**1a**−H_2O (5 mg, 6.4 μmol) was dissolved in degassed CH_2Cl_2 (5 mL). Degassed cumene (46.3 mmol, 5 mL) was added. The resulting solution was stirred for 10 min and then exposed to O_2. The orange solution turned black rapidly. After stirring for 1 h, the reaction mixture was analyzed by GC−MS to determine if any oxidation products of cumene were present (e.g., cumene hydroperoxide, cumenol, phenol); none were observed within the detection limits of the instrument.

Results and Discussion

Preliminary Observations. The colors of [Li]**1**−H_2O or [PPh_4]**1**−H_2O in water, acetonitrile, or methanol are orange to reddish orange. When [PPh_4]**1**−H_2O is dissolved in CH_2Cl_2 in the presence of O_2, the solution rapidly turns black with concomitant substantial changes in the UV/Vis spectrum. The black compound was found to react with PPh_3 to generate $OPPh_3$. UV/Vis, ^1H NMR, Mössbauer spectroscopy, labeling (^{18}O) experiments, and X-ray crystallographic analyses reveal that the reaction between the Fe^{III} of [PPh_4]**1**−H_2O and O_2 affords the remarkable dimeric μ-oxo diiron(IV) complexes **2** in high yields (Scheme 1).

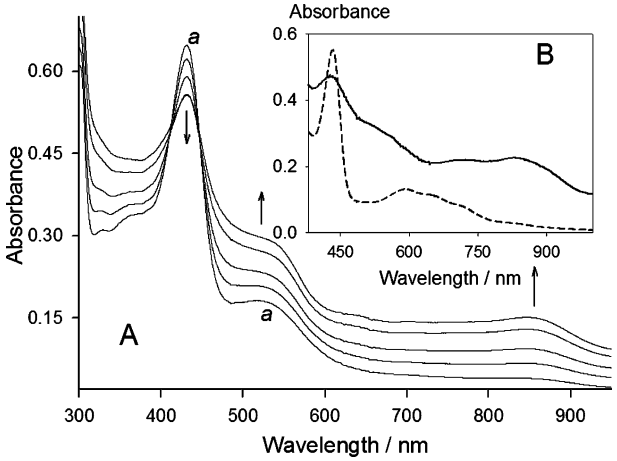

Figure 1. (A) UV/Vis analysis of the generation of **2a** from [PPh_4]**1a**−H_2O (7.71×10^{-5} M) and O_2 (ambient pressure) in dichloromethane at 24 °C; *a* is the spectrum at time $t = 0$; the sequential spectra were recorded at 2 min intervals. (B) UV/Vis spectra of [PPh_4]**1b**−H_2O (dotted line) and compound **2b** (solid line) in degassed CH_2Cl_2.

Synthesis of Complexes [PPh_4]1−H_2O and 2. [PPh_4]**1a**−H_2O and [PPh_4]**1b**−H_2O were synthesized by metathesis reactions of the lithium salts of **1** with excess [PPh_4]Cl in water. In contrast with the lithium salts of **1**, the tetraphenylphosphonium salt is sparingly soluble in water, allowing both [PPh_4]-**1a**−H_2O and [PPh_4]**1b**−H_2O to be obtained on precipitation in high yields. Complexes **2a** and **2b** were prepared by dissolving the corresponding tetraphenylphosphonium salts of **1a**−H_2O or **1b**−H_2O in CH_2Cl_2 and either leaving the solutions in the air for 10 min or bubbling in air or O_2. Both **2a** and **2b** were recrystallized as $[PPh_4]^+$ salts from a mixture of CH_2Cl_2 and α,α,α-trifluorotoluene. The isolated yields of these purified compounds were greater than 80%, and UV/Vis studies indicate that the conversions in solution are quantitative.

UV/Vis Spectroscopy of 2. The formation of **2** from [PPh_4]-**1**−H_2O can be followed by UV/Vis spectroscopy. When a degassed reddish solution of [PPh_4]**1a**−H_2O in CH_2Cl_2 is exposed to O_2, new bands form at 542 (ϵ 7500 M^{-1} cm^{-1}) and 856 nm (ϵ 5400 M^{-1} cm^{-1}) as the solution turns black; these bands indicate the formation of **2a** (Figure 1A). The intensity of the band at 431 nm from [PPh_4]**1a**−H_2O decreases. Isosbestic points at 413 and 447 nm suggest only **2a** is formed. Similarly, when a degassed solution of [PPh_4]**1b**−H_2O in CH_2Cl_2 (which is dark green in contrast with reddish [PPh_4]**1a**−H_2O in CH_2Cl_2) is exposed to O_2, black **2b** forms with new bands at 542 (ϵ 8800 M^{-1} cm^{-1}) and 856 nm (ϵ 6600 M^{-1} cm^{-1}) (Figure 1B). The similar spectral properties of **2a** and **2b** suggest common structural features. Thus far, complexes **2** have been generated only in aprotic weakly coordinating solvents, dichloromethane, trimethylacetonitrile, nitrobenzene, toluene, α,α,α-trifluorotoluene, 1,2-dichloroethane, 1,2-dichlorobenzene, and chloroform. Compounds **2a** and **2b** are stable for months in weakly

(51) Yamauchi, K.; Tanabe, T.; Kinoshita, M. *J. Org. Chem.* **1979**, *44*, 638−639.

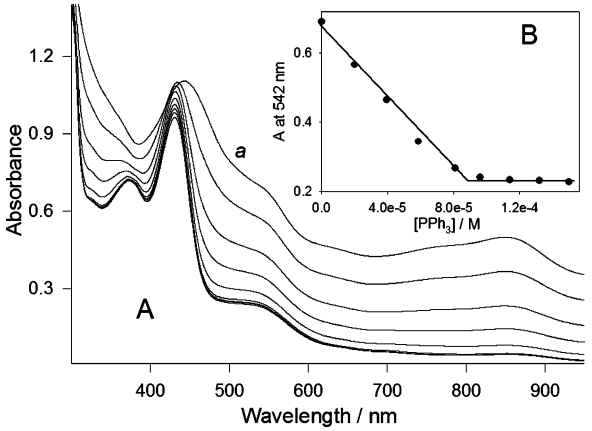

Figure 2. (A) Changes in the UV/Vis spectra upon incremental addition of PPh_3 to **2a** (9.2×10^{-5} M) in dichloromethane. Spectrum *a* was obtained at time $t = 0$. (B) Change of absorbance at 542 nm as a function of $[PPh_3]$.

coordinating chlorinated solvents. However, compounds **2** are not formed in better coordinating more nucleophilic solvents, such as water, methanol, or ethanol. Solid $[PPh_4]^+$ salts of **2a** and **2b** when dissolved in methanol or ethanol, quantitatively convert to the starting compounds within minutes at room temperature, as confirmed by UV/Vis spectroscopy and electrospray ionization mass spectrometry (ESI-MS).

Reaction of 2a with PPh_3 Monitored by UV/Vis Spectroscopy. Black **2a** reacts rapidly with PPh_3 at room temperature to afford $OPPh_3$ and **1a**, as confirmed by UV/Vis (Figure 2A), GC−MS, and Mössbauer spectroscopy and supported by ESI-MS. Such reactions of high-valent iron−oxo species with PPh_3 to generate $OPPh_3$ are known for both heme and non-heme Fe^{IV} complexes.[31,52] Consistent with the Fe^{IV} assignment, titration of **2a** with PPh_3 monitored by UV/Vis spectroscopy requires 1 equiv of PPh_3, and correspondingly 1 equiv of $OPPh_3$ is generated (GC−MS analysis) (Figure 2B). Compound **2b** also reacts with PPh_3 to afford **1b** and $OPPh_3$. Aerial oxidation of PPh_3 by O_2 is slow. When more than 1 equiv of PPh_3 is added to **1a** at room temperature, the binding of $OPPh_3$ and/or excess PPh_3 to **1a** apparently inhibits regeneration to **2a** by O_2. When degassed CH_2Cl_2 solutions of either PPh_3 or $OPPh_3$ and $[PPh_4]$-**1a**$-H_2O$ are mixed, a decrease in the band at 431 nm for the iron complex is observed and a new band at 372 nm is generated. Similar changes are observed during the titration of **2a** with PPh_3. The Mössbauer spectrum of **2a** following its titration with PPh_3 revealed the presence of multiple Fe^{III} species, also suggesting that both PPh_3 and $OPPh_3$ bind to **1a**. However, compound **2a** does re-form on prolonged standing at room temperature (UV/Vis evidence), and the addition of further PPh_3 results in ongoing conversion to $OPPh_3$.

Mössbauer Spectroscopy. The Mössbauer spectra of solid **2a** obtained at 4.2 K reveal the rare high-valent character of the iron centers (Figure 3). The zero field spectrum (Figure 3A) consists of one doublet with quadrupole splitting, $\Delta E_Q = 3.3$ mm/s, and isomer shift (vs Fe metal at 298 K), $\delta = -0.07$ mm/s. These parameters are characteristic of an $S = 1$ Fe^{IV} site.[53] The Mössbauer data do not exclude the possibility that the local sites of **2** are high-spin ($S = 2$) Fe^{IV}. However, all known high-spin Fe^{IV} complexes have $|\Delta E_Q| < 1$ mm/s. In contrast, most S

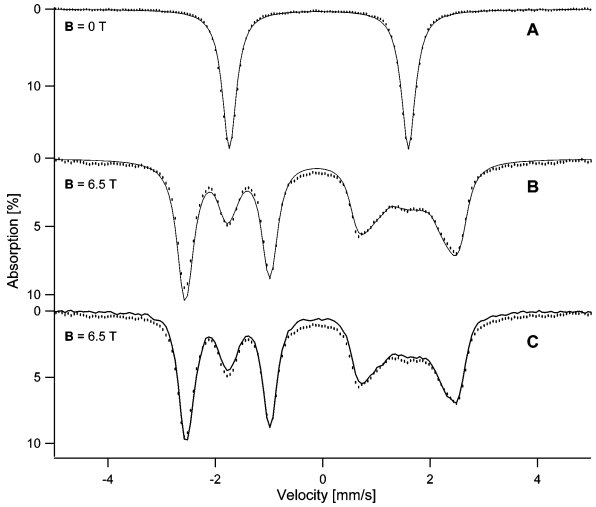

Figure 3. The 4.2 K Mössbauer spectra of solid **2a** recorded in zero field (A) and in a 6.5 T field applied parallel to the γ-beam (B). The solid lines are spectral simulations assuming a diamagnetic ground state. The simulations yield $\Delta E_Q > 0$ and the asymmetry parameter $\eta = 0.15 \pm 0.15$. The sample contained a ferric contaminant (5% of total Fe), perhaps some unreacted $[PPh_4]$**1a**$-H_2O$. (C) Comparison of two 6.5 T spectra of the *n*-butyronitrile sample recorded at 4.2 and 80 K.

$= 1$ Fe^{IV} complexes exhibit substantially larger ΔE_Q values, up to 3.5 mm/s.[20,44b,54,55] Such sites generally exhibit substantial paramagnetic hyperfine structure when examined in applied magnetic fields at 4.2 K. The 6.5 T spectrum of **2a** (Figure 3B), in contrast, reveals a diamagnetic site, suggesting that **2a** is an antiferromagnetically coupled ($H = J\mathbf{S}_1\bullet\mathbf{S}_2$, $J > 0$) bis-iron(IV) dinuclear species. The solid line in Figure 3B is a spectral simulation assuming that the iron of **2a** resides in a diamagnetic ($S = 0$) environment. The simulation confirms the diamagnetism of the site, and it yields $\Delta E_Q > 0$ and $\eta = 0.15$ for the asymmetry parameter η of the electric field gradient tensor. A 6.5 T spectrum of **2a** dissolved in *n*-butyronitrile (95% ^{57}Fe) was identical to that observed in the solid. Mössbauer spectroscopy can be used to measure the exchange coupling constant J, provided $J < 120$ cm^{-1}.[56,57] Figure 3C compares two 6.5 T spectra of the *n*-butyronitrile sample recorded at 4.2 and 80 K. It can be seen that the magnetic splittings at both temperatures are essentially identical, showing that excited states of the spin ladder (e.g., $S = 1$) are not measurably populated at this temperature. This observation indicates that $J > 100$ cm^{-1}. The Mössbauer spectra of **2b** are quite similar to those of **2a**; for **2b**, we observed $\Delta E_Q = 3.00$ mm/s and $\delta = -0.03$ mm/s at 4.2 K. While the Mössbauer spectra of **2a** place a lower limit of 100 cm^{-1} on J, the room temperature ^1H NMR spectra suggest that the exchange coupling constant J is substantially larger. Thus, the signals from $NC(CH_3)_2CO$ protons (12 in total) appear as a singlet at δ 1.54 in the metal-free ligand of **1a**. These groups become diastereotopic in dimers **2a** (or **2b**), and

(52) Rohde, J.-U.; In, J.-H.; Lim, M. H.; Brennessel, W. W.; Bukowski, M. R.; Stubna, A.; Münck, E.; Nam, W.; Que, L., Jr. *Science* **2003**, *299*, 1037−1039.
(53) Lim, M. H.; Rohde, J.-U.; Stubna, A.; Bukowski, M. R.; Costas, M.; Ho, R. Y. N.; Münck, E.; Nam, W.; Que, L., Jr. *Proc. Natl. Acad. Sci. U.S.A.* **2003**, *100*, 3665−3670.
(54) Zheng, H.; Yoo, S. J.; Münck, E.; Que, L., Jr. *J. Am. Chem. Soc.* **2000**, *122*, 3789−3790.
(55) Dong, Y.; Que, L., Jr.; Kauffmann, K.; Münck, E. *J. Am. Chem. Soc.* **1995**, *117*, 11377−11378.
(56) Kauffmann, K. E.; Münck, E. In *ACS Symposium on Spectroscopic Methods in Bioinorganic Chemistry*; Solomon, E. I., Hodgson, K. O., Eds.; American Chemical Society: Washington, DC, 1998; pp 16−29.
(57) Krebs, C.; Bollinger, J. M., Jr.; Theil, E. C.; Huynh, B. H. *J. Biol. Inorg. Chem.* **2002**, *7* (7−8), 863−869.

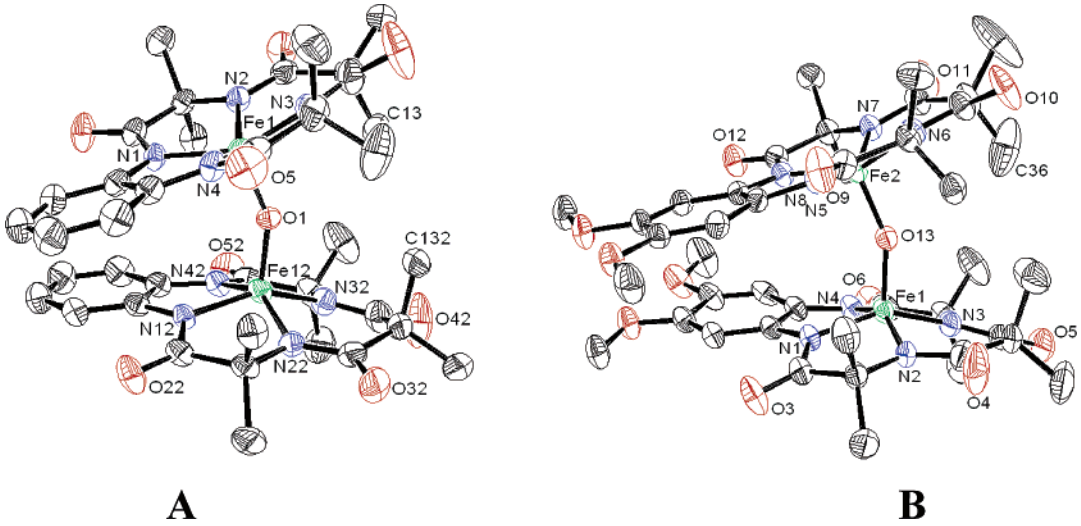

Figure 4. ORTEP structures of complexes **2a** (A) and **2b** (B). The ellipsoids are drawn at the 50% probability level.

Table 2. Selected Bond Distances (Å) and Bond Angles (deg) for **2a** and **2b**

	2a	2b
Fe(1)−Fe(2)	3.3497(9)	3.3834(8)
Fe(1)−O(1)	1.7284(8)	
Fe(1)−O(13)		1.744(3)
Fe(2)−O(13)		1.730(2)
Fe(1)−N(1)	1.875(2)	1.881(4)
Fe(1)−N(2)	1.896(2)	1.903(3)
Fe(1)−N(3)	1.903(3)	1.904(3)
Fe(1)−N(4)	1.875(2)	1.877(3)
Fe(2)−N(5)		1.870(3)
Fe(2)−N(6)		1.904(4)
Fe(2)−N(7)		1.903(4)
Fe(2)−N(8)		1.888(3)
Fe(1)−O(1)−Fe(1)	151.4(2)	
Fe(1)−O(13)−Fe(2)		153.8(2)
O(1)−Fe(1)−N(1)	104.4(1)	
O(1)−Fe(1)−N(2)	104.16(7)	
O(1)−Fe(1)−N(3)	105.5(1)	
O(1)−Fe(1)−N(4)	107.52(8)	
O(13)−Fe(1)−N(1)		107.7(1)
O(13)−Fe(1)−N(2)		106.5(1)
O(13)−Fe(1)−N(3)		104.2(1)
O(13)−Fe(1)−N(4)		102.9(1)
O(13)−Fe(2)−N(5)		102.8(1)
O(13)−Fe(2)−N(6)		103.4(1)
O(13)−Fe(2)−N(7)		107.8(1)
O(13)−Fe(2)−N(8)		106.9(1)
N(1)−Fe(1)−N(2)	84.11(10)	83.5(1)
N(1)−Fe(1)−N(3)	149.4(1)	147.1(1)
N(1)−Fe(1)−N(4)	81.6(1)	81.2(1)
N(2)−Fe(1)−N(3)	94.6(1)	95.3(1)
N(2)−Fe(1)−N(4)	147.6(1)	149.81(2)
N(3)−Fe(1)−N(4)	83.5(1)	83.9(1)
N(5)−Fe(2)−N(6)		84.0(1)
N(5)−Fe(2)−N(7)		148.7(1)
N(5)−Fe(2)−N(8)		81.3(1)
N(6)−Fe(2)−N(7)		95.2(1)
N(6)−Fe(2)−N(8)		148.6(1)
N(7)−Fe(2)−N(8)		83.6(1)

two singlet resonances are observed for the 24 methyl protons of the five-membered rings. The present ^{1}H NMR information cannot be used to infer a lower limit of J as the ^{1}H NMR data and J values of other Fe^{IV}−TAML complexes have not been reported. However, the paramagnetic proton shifts of Fe^{IV} porphyrins are typically 10 times larger than the shifts observed here.

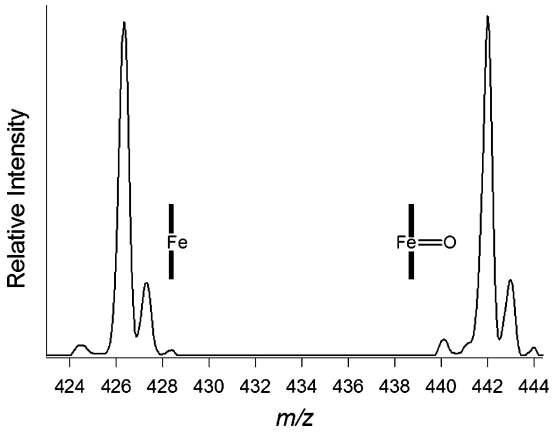

Figure 5. ESI-MS of **2a** dissolved in CH_2Cl_2 showing its disproportionation into **1a** and **1a**(O).

X-ray Crystallographic Analysis of 2a and 2b. X-ray crystallographic studies demonstrate that both **2a** and **2b** are bis(Fe^{IV})-μ-oxo complexes (Figure 4). Selected bond distances and angles are listed in Table 2. Each Fe^{IV} center is coordinated by four deprotonated amide nitrogens and the axial bridging oxo ligand. The average Fe−N bond distances in **2a** (1.887(12) Å) and **2b** (1.891(13) Å) are comparable to the reported distances for Fe^{III} and Fe^{IV} mononuclear TAML complexes.[44a,b,45] The mean deviation of each iron atom from the 4N plane in **2a** and **2b** equals 0.50 Å. This is longer than that in [PPh$_4$]**1a**−H_2O (0.36 Å), but comparable to that in other closely related Fe^{IV}−TAML complexes.[44a,b,45] The Fe−O bond distances in **2a** (1.7284(8) Å) and **2b** (1.744(3) and 1.730(2) Å) are shorter than those in the bis(μ-oxo)-bridged complexes, Fe^{IV}(O)$_2$Fe^{IV} (1.79 Å)[58] and Fe^{III}(O)$_2$Fe^{IV} (1.80 and 1.860 Å).[59] The Fe−O distance in **2a** is slightly shorter than the average (1.77 Å) reported for that in the μ-oxo-bridged Fe^{III} compounds.[60] Consideration of

(58) Costas, M. L.; Rohde, J.-U.; Stubna, A.; Ho, R. Y. N.; Quaroni, L.; Münck, E.; Que, L., Jr. *J. Am. Chem. Soc.* **2001**, *123*, 12931−12932. Subsequent work in the Que and Münck laboratories has shown that the complex of Costas et al. was incorrectly identified to have an Fe_2O_2 core. It is, in fact, a novel monomeric Fe^{IV} peroxo complex (Jensen, M. P.; Costas, M.; Ho, R. Y. N.; Kaizer, J.; Mairata i Payeras, A.; Münck, E.; Que, L., Jr.; Rohde, J.-U.; Stubna, A. Submitted).
(59) Hsu, H.-F.; Dong, Y.; Shu, L.; Young, V. G., Jr.; Que, L., Jr. *J. Am. Chem. Soc.* **1999**, *121*, 5230−5237.
(60) Kurtz, D. M., Jr. *Chem. Rev.* **1990**, *90*, 585−606.

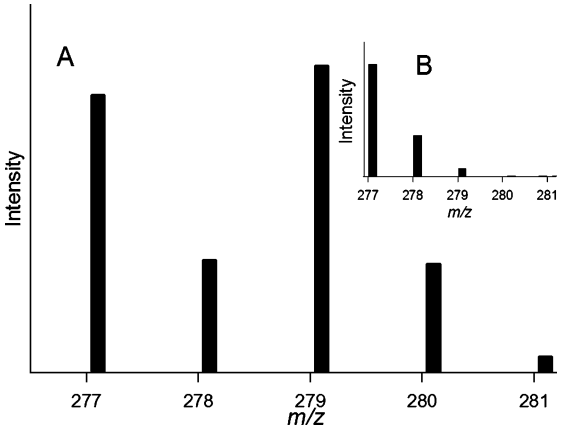

Figure 6. (A) Mass spectrum of $^{18}OPPh_3$ [$(M - 1)^+$ peak is shown]. Compound **2a** was prepared by reacting $^{18}O_2$ and [PPh_4]**1a**$-H_2O$; it was then reacted with PPh_3. GC−MS analysis of the product showed the incorporation of 53% ^{18}O isotope in $OPPh_3$. (B) Mass spectrum of $^{16}OPPh_3$ is shown for comparison.

the orbital occupancies of the π-bonding system of the $Fe^{IV}-O-Fe^{IV}$ unit suggests that the formal bond order between each Fe^{IV} and the oxo ligand should be two. Nevertheless, it is not surprising that the Fe−O bond distances in **2a** and **2b** are similar to those in the $Fe^{III}-O-Fe^{III}$ systems. The four strongly σ-donating deprotonated amide ligands always noticeably weaken axial ligand bonding often resulting in the rejection of axial ligands leading to lower coordination numbers.[38] The Fe−O bond distances in **2a** and **2b** are significantly longer than the Fe=O distances in various protein and synthetic Fe^{IV}=O heme derivatives (1.60−1.69 Å, EXAFS)[61−63] or non-heme mononuclear Fe^{IV}=O complexes of tetradentate-N4 macrocyclic and tripodal ligands (1.65−1.67 Å, X-ray and EXAFS).[52,53] The Fe−O distances in **2a** and **2b** are shorter than the terminal $Fe^{III}-O$ bond distance (1.813 ± 0.003 Å) of Borovik's novel iron(III)−monooxo complex;[28] presumably the higher oxidation state of iron in **2** is significantly responsible. The $Fe^{IV}-O-Fe^{IV}$ bond angles in **2** are in the range of 151.4(2)−153.8(2)° and are comparable to reported $Fe^{III}-O-Fe^{III}$ bond angles.[60] The planes defined by the four N atoms surrounding the iron(IV) sites are tilted toward the benzene rings, perhaps to avoid steric crowding of the methyl groups at the six-membered rings. There is a short C13···O1 contact in complex **2a** suggesting an intramolecular hydrogen bond between the bridging oxygen and the corresponding hydrogen at C13; the C−H···O1 separation is 2.319 Å.

Electrospray Ionization Mass Spectra (ESI-MS). Intact **2a** and **2b** dimers could not be detected in ESI-MS experiments (calculated *m*/*z* 434 for **2a** and *m*/*z* 494 for **2b**). Instead, two peaks of similar abundance were observed with *m*/*z* 426 and 442 for **2a** (Figure 6) and *m*/*z* 486 and 502 for **2b**. The *m*/*z* values and the isotopic patterns for the 426 and 486 peaks correspond to **1a** (*m*/*z* 426) and **1b** (*m*/*z* 486), while those for the 442 and 502 peaks fit to the oxo complexes, **1a**(O) (*m*/*z* 442) and **1b**(O) (*m*/*z* 502). These results suggest that **2** disproportionates in the ESI-MS interface giving **1** and **1**(O) (Scheme 2).

Scheme 2. Summary of the ^{18}O Isotope Labeling Pathways and Related Experiments

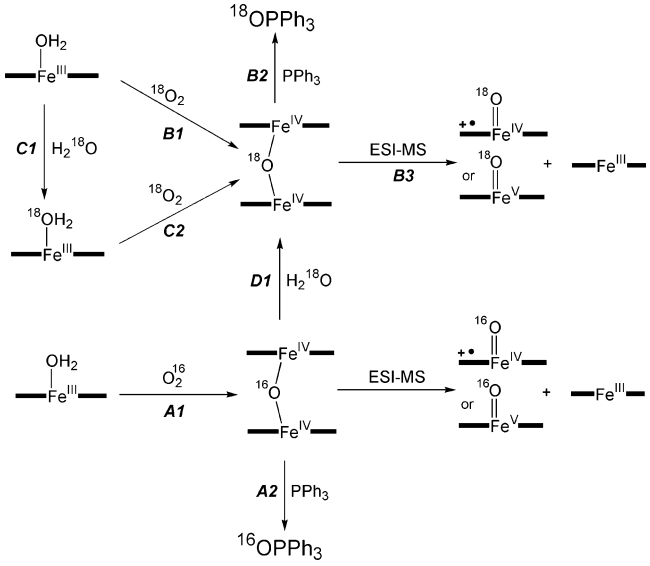

Origin of the Oxo Ligand. Complexes **2** are produced when solutions of [PPh_4]**1**$-H_2O$ are exposed to O_2. The reaction between **2a** and PPh_3 that affords **1a** and $OPPh_3$ was used to confirm that the bridging μ-oxo ligand originates from O_2 in the following way. Compound [PPh_4]**1a**$-H_2O$ was first treated with 90% enriched $^{18}O_2$ in degassed CH_2Cl_2 to generate **2a** (pathway B1 in Scheme 2). A portion of the reaction mixture was analyzed by ESI-MS, and 31% ^{18}O enrichment was found (**2a** decomposes via pathway B3 of Scheme 2 in the ESI-MS interface). The remainder of the reaction mixture was reacted with PPh_3 (pathway B2). The $OPPh_3$ product was found to contain 53% enrichment in ^{18}O (Figure 6). The difference in ^{18}O incorporation found for **2a** compared with $OPPh_3$ produced from **2a** arises from a rapid O exchange between ^{18}O−**2a** and traces of $H_2{}^{16}O$. In the experiments described above, $H_2{}^{16}O$ was always present as the axial ligand in [PPh_4]**1a**$-H_2O$ and as a solvent contaminant. Introduction of traces of water in compound manipulations could provide additional sources of ^{16}O. The difference found in the ^{18}O level of **2a** and derived $OPPh_3$ signifies a high sensitivity to trace water with different samples' exposures to adventitious water during the analyses. Exchange of the O atoms of iron oxo ligands with water is well documented and has been used as indirect evidence for the existence of high-valent oxometal species.[64−69] Here, experimental proof for the rapid **2a**$-O/H_2O$ exchange was obtained. [PPh_4]**1a**$-H_2O$ was stirred with $H_2{}^{18}O$ (95%) in acetonitrile for 3 h, and the solvent was then removed in vacuo (pathway C1 in Scheme 2). The ^{18}O-enriched complex [PPh_4]**1a**$-H_2{}^{18}O$ was then treated with $^{18}O_2$ in CH_2Cl_2 to give **2a** (pathway C2), which was again immediately reacted with PPh_3 (B2). The ^{18}O

(61) Penner-Hahn, J. E.; Able, K. S.; McMurry, T. J.; Renner, M.; Balch, A. L.; Groves, J. T.; Dawson, J. H.; Hodgson, K. O. *J. Am. Chem. Soc.* **1986**, *108*, 7819−7825.
(62) Wolter, T.; Meyer-Klaucke, W.; Muther, M.; Mandon, D.; Winkler, H.; Trautwein, A. X.; Weiss, R. *J. Inorg. Biochem.* **2000**, *78*, 117−122.
(63) Chance, M.; Powers, L.; Poulos, T.; Chance, B. *Biochemistry* **1986**, *25*, 1266−1270.
(64) Goh, Y. M.; Nam, W. *Inorg. Chem.* **1999**, *38*, 914−920.
(65) Nam, W.; Valentine, J. S. *J. Am. Chem. Soc.* **1993**, *115*, 1772−1778.
(66) Bernadou, J.; Meunier, B. *Chem. Commun.* **1998**, 2167−2173.
(67) Balahura, R. J.; Sorokin, A.; Bernadou, J.; Meunier, B. *Inorg. Chem.* **1997**, *36*, 3488−3492.
(68) Song, R.; Sorokin, A.; Bernadou, J.; Meunier, B. *J. Org. Chem.* **1997**, *62*, 673−678.
(69) (a) Pitie, M.; Bernadou, J.; Meunier, B. *J. Am. Chem. Soc.* **1995**, *117*, 2935−2936. (b) Bernadou, J.; Fabiano, A.-S.; Robert, A.; Meunier, B. *J. Am. Chem. Soc.* **1994**, *116*, 9375−9376.

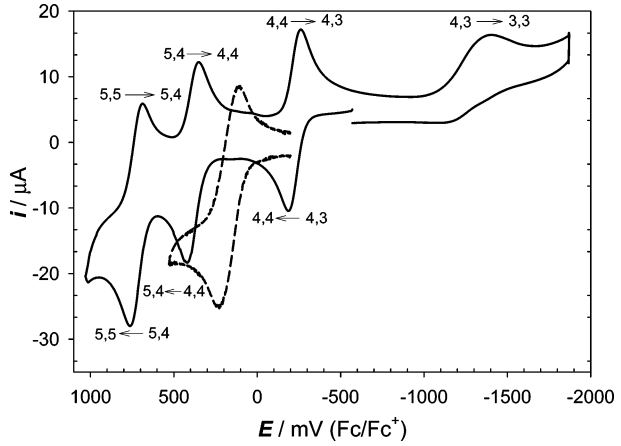

Figure 7. Cyclic voltammograms of [PPh4]**1a**−H_2O (dashed line, 9×10^{-4} M) and **2a** (solid line, 6.4×10^{-4} M) in dichloromethane (0.1 M *n*-tetrabutylammonium perchlorate), a glassy carbon working electrode, scan rate of 50 mV s^{-1}. Assignments of formal oxidation states are made to suggest either the indicated state or alternatives where the oxidation(s) is from the TAML ligand(s).

enrichment of the resulting $OPPh_3$ was 86%. The ^{18}O-enriched complex [PPh_4]**1a**−$H_2{}^{18}O$ was also reacted with $^{16}O_2$, and the product was examined by ESI-MS to reveal 44% ^{18}O enrichment of **2a**. Finally, a solution of **2a** in CH_2Cl_2 containing oxygen isotopes in natural abundance was treated with $H_2{}^{18}O$ (95%) for 3 h (pathway D1). The resulting **2a** was reacted with PPh_3 to give 73% $^{18}OPPh_3$. These data clearly indicate that the μ-oxo ligand comes from dioxygen, but is subject to rapid oxygen atom exchange with water. As known,[70] the exchange process has to be quite complicated involving, at a minimum, cleavage and reformation of Fe−O bonds to two Fe^{IV} centers (four bonds in all involved, two Fe−^{16}O and two Fe−^{18}O), various coordinations of water ligands to both sites, and appropriate redistribution of protons.

Generation of 2 in the Presence of Cumene. Apart from direct interaction between [PPh_4]**1**−H_2O and O_2, trace organic peroxides present in organic solvents or other adventitious radicals could initiate free radical autoxidation of complexes [PPh_4]**1**−H_2O into **2**.[71] However, this is unlikely because **2a** is rapidly and quantitatively generated in a variety of commercial high purity chlorinated and non-chlorinated solvents, which were additionally purified to remove peroxides. To further probe for solvent-mediated radical pathways, **2a** (6 μmol) was generated in the presence of cumene (0.046 mol, cumene:CH_2Cl_2 = 1:1 v/v). Because of its weak tertiary C−H bond, cumene readily participates in free radical autoxidation processes, and indeed, this is the basis of the commercial production of cumene hydroperoxide. No oxidation products of cumene were observed by GC−MS, suggesting that the Fe^{IV}−O−Fe^{IV} formation does not involve solvent-mediated free radical autoxidation chemistry.

Cyclic Voltammetry of 2a and 2b. Electrochemical characteristics of [PPh_4]**1**−H_2O and **2** derived from cyclic voltammetry reflect the dinuclear nature of **2**. Both mononuclear starting materials, [PPh_4]**1a**−H_2O and [PPh_4]**1b**−H_2O, show a single electrochemically reversible redox process at $E_{1/2} = 0.17$ (Figure 7) and −0.18 V versus Fc/Fc^+, respectively, corresponding to a one-electron oxidation.[72] Dinuclear **2a** exhibits three electrochemically reversible features (Figure 7) at $E_{1/2}$ = −0.23 (ΔE_p = 77), 0.37 (68), and 0.72 V (74 mV) and one irreversible reduction, $E_{p,red}$ at −1.30 V. Complex **2b** shows three reversible processes at $E_{1/2} = -0.67$ ($\Delta E_p = 111$), −0.15 (101), and 0.30 V (111 mV) versus Fc/Fc^+. Decamethylferrocene reduces **2a** by one electron (UV/Vis titration) giving the mixed-valent dinuclear species. This suggests that the feature at −0.23 V for **2a** should be ascribed to the $Fe^{IV}OFe^{IV}$ to Fe^{III}-OFe^{IV} transformation. The tentative assignments for the other redox processes of **2a** are shown in Figure 7.

Mechanistic Consideration. Two decades ago, Balch and co-workers[29,30] analyzed the formation of dinuclear PFe^{III}−O−$Fe^{III}P$ (P = porphyrin) compounds from ferrous porphyrins and O_2. The reactions proceed through peroxo-bridged diferric intermediates, PFe^{III}−O_2−$Fe^{III}P$, that decay via O−O bond cleavage into reactive PFe^{IV}=O species. The latter then reacts with PFe^{II}, PFe^{III}−O_2−$Fe^{III}P$, or $PFe^{II}(O_2)$ to form the final product, PFe^{III}−O−$Fe^{III}P$. The reversible oxidations observed in the electrochemical studies of **2** indicate that **2** is easily oxidized. Thus, we envision that the **2** complexes are produced via a mechanism similar to that of the μ-oxo-diferric porphyrins, except that all the species involved exist in oxidation states that are one unit higher than their porphyrin analogues (Figure 8).

Reactivity of 2a. It has been shown that **2a** and **2b** catalytically oxidize PPh_3 into $OPPh_3$. Oxidation of alcohols to the corresponding aldehydes, ketones, and carboxylic acids is an important synthetic reaction.[73] The most commonly used oxidants are toxic chromium compounds.[74] Several green alternative reagents have been proposed,[75] including transition metal catalysts that use dioxygen.[76] We have found that the **2** compounds catalyze the oxidation of benzylic alcohols (benzyl, 4-chlorobenzyl, 4-nitrobenzyl, 4-methoxybenzyl, cinnamyl) by O_2 into the corresponding aldehydes in 1,2-dichlorobenzene or nitrobenzene at 100 °C. The highest conversion thus far involves transformation of 60 equiv of benzyl alcohol to benzaldehyde per equivalent of **2a** within 1 h without production of benzoic acid. As the alcohols are oxidized, **2a** returns to **1a** (UV/Vis and ESI-MS characterization). The oxidation also occurs at 40−50 °C where benzyl alcohol is oxidized to benzaldehyde in 3−4 h. Benzyl alcohol reacts slowly with **2a** at room temperature over 12−16 h. The oxidation of alcohols was also achieved by in situ generation of **2a** from [PPh_4]**1a**−H_2O in 1,2-dichlorobenzene with subsequent addition of alcohols. When complex **2a**, dissolved in acetone or acetonitrile, is added to an aqueous solution of Orange II, a rapid bleaching of this commercial dye occurs. The bleaching of Orange II by **2a** is very fast, and the initial rate is comparable to that found when Orange II is catalytically bleached in water by H_2O_2 in the presence of **1**−H_2O.[77] The bleaching by complexes **2** is not catalytic under

(70) Seo, M. S.; In, J.-H.; Kim, S. O.; Oh, N. Y.; Hong, J.; Kim, J.; Que, L., Jr.; Nam, W. *Angew. Chem., Int. Ed.* **2004**, *43*, 2417−2420.
(71) Valentine, J. S. In *Bioinorganic Chemistry*; Bertini, I., Gray, H. B., Lippard, S. J., Valentine, J. S., Eds.; University Science Books: Mill Valley, CA, 1994; pp 252−313.
(72) Uffelman, E. S. Ph.D. Thesis, California Institute of Technology, Pasadena, California, 1992.
(73) Hudlicky, M. In *Oxidations in Organic Chemistry*; American Chemical Society: Washington, DC, 1990.
(74) Cainelli, G.; Cardillo, G. *Chromium Oxidations in Organic Chemistry*; Springer: Berlin, 1984.
(75) Sheldon, R. A.; Arends, I. W. C. E.; ten Brink, G.-j.; Dijksman, A. *Acc. Chem. Res.* **2002**, *35*, 774−781.
(76) Sheldon, R. A.; Arends, I. W. C. E. In *Advances in Catalytic Activation of Dioxygen by Metal Complexes*; Kluwer Academic Publishers: Dordrecht/Boston/London, 2003; Vol. 26, pp 123−155.
(77) The mechanistic details of this study will soon be submitted: Ghosh, A.; Mitchell, D. A.; Ryabov, A. D.; Popescu, D. L.; Upham, E.; Hangun, Y.; Alexandrova, L.; Collins, T. J.. The exact structure of the high-valent fragment is currently under investigation.

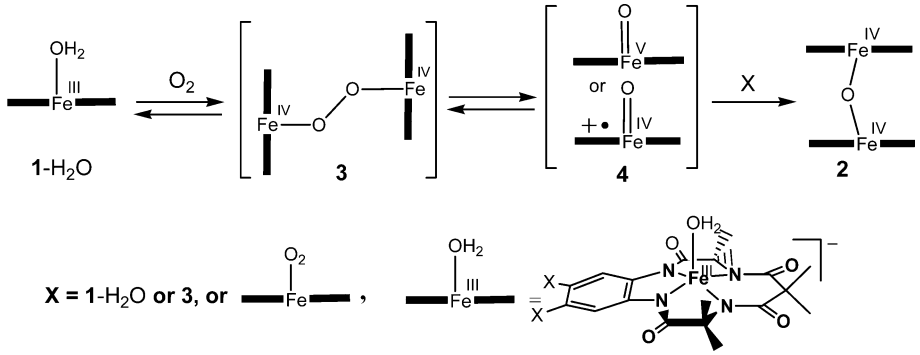

Figure 8. Proposed mechanism for the formation of **2** from $[PPh_4]$**1**$-H_2O$ and O_2.

these conditions. Efforts are currently underway to expand the scope of catalytic oxidations of organic compounds by dioxygen in the presence of complexes **1** or **2** and to identify the reactive species generated from complexes **2** in water. Interestingly, the preliminary data suggest that one and the same reactive intermediate is produced when **1** reacts with H_2O_2 in water or when complexes **2** are first made from **1** and O_2 in CH_2Cl_2 and then treated with water.

Conclusions

The direct activation of dioxygen by an iron(III) center in a coordination compound has been demonstrated. This is unprecedented behavior for an iron(III) complex toward dioxygen. Previously, only iron(II) coordination compounds were found to react directly with O_2 to afford high-valent oxo−iron species. This distinctive feature of Fe^{III}−TAML complexes is a consequence of the presence of the four strongly donating amidato nitrogens. These stabilize to a great extent the oxidized metal centers relative to more common ligand systems. The Fe^{IV}−O−Fe^{IV} complexes are capable of catalytically oxidizing various substrates in the presence of dioxygen. The oxidation types observed thus far include formal oxygen atom transfer reactions (PPh_3/Ph_3PO) and two electron-transfer-type reactions (alcohol to aldehyde).

This new reaction type for iron and O_2 involves both the principal biochemical oxidizing agent and the principal catalytic metal of biochemical oxidation processes. Therefore, if the catalytic performance of **1**$-H_2O$ can be expanded to a broader variety of substrates and improved in terms of rates and turnover numbers, the approach could provide an industrially appealing method for moving the elemental composition of industrial homogeneous oxidation processes toward the elemental composition of biochemistry. Bringing about such a movement is the best way to reduce the production of persistent bioaccumulative pollutants that accompany many incumbent oxidation technologies.[1]

Acknowledgment. We thank the Eden Hall Foundation, the Charles Edison Foundation, the DOE, the Institute for Green Oxidation Chemistry of CMU (T.J.C.), and the NSF (E.M.) for financial support, the Heinz Foundation for the Award of a Teresa Heinz Environmental Scholarship (A.G.), the NSF for the award of a Predoctoral Fellowship (E.S.B.), and Arani Chanda for obtaining spectral data.

Supporting Information Available: ESI-MS and GC−MS spectral data for isotope labeling experiments of **2a** (ESI-MS) and its PPh_3 (GC−MS) reaction product (Figures S3−S6). ^1H NMR spectra, UV/Vis titration spectra for **2a** with Cp^*_2Fe and the bleaching of Orange II (Figures S1, S2, and S7), and X-ray crystallographic files (CIF). This material is available free of charge via the Internet at http://pubs.acs.org.

JA0460458